INTERNATIONAL JOURNAL OF SUSTAINABLE CONSTRUCTION ENGINEERING AND TECHNOLOGY
Vol. 11 No. 4 (2021) 8-17

© Universiti Tun Hussein Onn Malaysia Publisher's Office

IJSCET

http://penerbit.uthm.edu.my/ojs/index.php/ijscet
ISSN : 2180-3242 e-ISSN : 2600-7959

International Journal of Sustainable Construction Engineering and Technology

Determination of the Bearing Capacity of Concrete-Filled Steel Tubular Structures Coupled with Dismountable Joints

P. Semko[1], G. Gasii[2*]

[1]Poltava National Technical Yuri Kondratyuk University,
Pershotravnevyj Ave. 24, Poltava, 36011, UKRAINE

[2]Sumy National Agrarian University,
160 Herasym Kondratiev, Sumy, 40021, UKRAINE

*Corresponding Author

DOI: https://doi.org/10.30880/ijscet.2021.11.04.002
Received 07 august 2019; Accepted 15 December 2020; Available online 31 December 2020

Abstract: The analysis method of the bearing capacity of concrete-filled steel tubular structures coupled with dismountable joints is presented (in particular elements with flange joints, and longitudinal ribs joints, and steel coupling joints). With the help of the above way, the curves of the bearing capacity of the dismountable joints are plotted. The comparison was made to determine the most optimal joints from presented.

Keywords: Concrete-filled tubular element, bearing capacity, dismountable joint

1. Introduction

Commencing as building constructions around a century ago, concrete-filled tubular structures have lately become more and more widespread in various fields of construction, including civil construction (Fam, A., Qie, F. S., & Rizkalla, S., 2004; Hancock, G., Wilkinson, T. J., & Zhao, X. L., 2005 and Hudz, S., et al.,2018). This is explained by the efficiency grouping of steel and concrete, thanks to that concrete-filled tubular structures have high strength, durability, reliability, meet high-tech requirements at relatively low material costs (Semko, P., 2018 and Semko, P., Skliarenko, S., & Semko, V., 2018). However, the most important and challenging issue in concrete structures designing is the question of the implementation of joints (Gasii, G. M., 2014). Frequently as mounting of structures large bending moments occur in the joints. In current work, the method of determination of bending moments, as well as comparing different designs of dismountable joints of concrete-filled tubular elements for both bearing capacity, and materials costs are presented (on the example of a real structure of a shopping mall) (Zeghiche, J., & Chaoui, K., 2005; Gasii, G., Hasii, O., & Zabolotskyi, O., 2017; Tao, Z. et al 2016; Gasii G. M., 2017 and Kolokhov, V., et al., 2018).

2. The Investigation Results

Grounded on the hypothesis of Bernoulli (hypothesis of plane cross sections), particularly, the thesis on the equality of strains within an element and on its surface, will be defined the characteristics of the stress-strain state of the sample of the concrete-filled tubular element of 108 mm in diameter and 4 mm in thickness of wall. To do this needs to follow the steps (Lai, M. H., & Ho, J. C. M., 2016). The concrete element is broken down to 27 identical sections (see Fig. 1), and their geometric parameters are defined (in particular, the area of the site and the location of the center of gravity) by the formulas (1–4).

*Corresponding author: grigoriigm@gmail.com

2021 UTHM Publisher. All rights reserved.

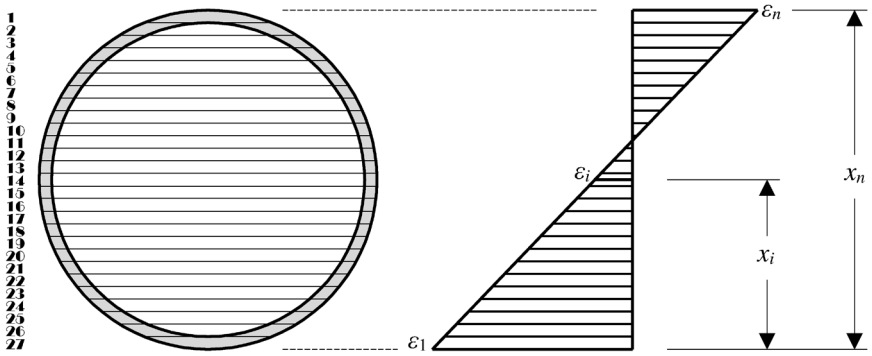

Fig. 1 - Dividing the concrete-filled tubular element into plots.

The overall area of the first plot is calculated with the following formula:

$$A_{c,seg\,i} = 0{,}5r^2 \cdot (\pi \cdot \frac{\alpha}{180} - \sin(\alpha)) \quad (1)$$

where α – an angle of an arc of i-th segment, and r – an arc radius of i-th segment.

The area of a steel tube (Fam, Qie & Rizkalla, 2004), for the corresponding i-th segment is calculated with the following formula:

$$A_{s,seg\,i} = 0{,}5R^2 \cdot (\pi \cdot \frac{\alpha}{180} - \sin(\alpha)) - 0{,}5r^2 \cdot (\pi \cdot \frac{\alpha}{180} - \sin(\alpha)) \quad (2)$$

The area of the i-th concrete segment is calculated with the following formula:

$$A_i = A_{seg\,i} - A_{seg\,i-1} \quad (3)$$

Coordinates of the point of gravity are calculated with the following formula:

$$y_i = \frac{(2 \cdot r \cdot \sin(\alpha/2))^3}{12 A_{c,seg\,i}} \quad (4)$$

As the boundary conditions for both first and last plots (see Table 1), strains were reached corresponding to the strains of the yield strength of the steel (compression of the first section, and bend of the last). The strain of each i-th section (see Fig. 1) is calculated with the following formula:

$$\varepsilon_i = \frac{(\varepsilon_1 - \varepsilon_n)}{x_n \cdot x_i} + \varepsilon_n \quad (5)$$

Grounded on the values of the strains of each i-th section, the corresponding values of stresses for each of the sections (separately steel and concrete) are calculated with the following formulas:

$$\varepsilon_i \geq \varepsilon_{c3}, \sigma_c = f_{cm} \quad (6)$$

$$\varepsilon_i \leq \varepsilon_{c3}, \sigma_c = E_{cm} \cdot \varepsilon_i \quad (7)$$

$$\varepsilon_y \geq f_y, \sigma_y = E_s \cdot \varepsilon_i \quad (8)$$

Table 1 - Boundary conditions to plotting *N–M* diagram.

№	ε_1	ε_n	Diagram
1 (axial compression)	$-f_y / E$	$-f_y / E$	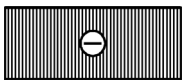
2	$-f_y / E$	$-0{,}5 \times f_y / E$	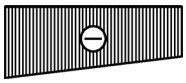
3	$-f_y / E$	$0{,}5 \times f_y / E$	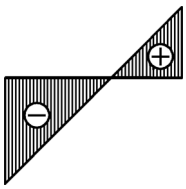
4	$-f_y / E$	f_y / E	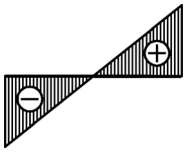
5 (bending)	$-k \times f_y / E$	f_y / E	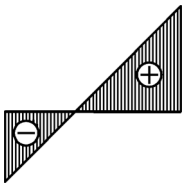

Then, needs to find the values of the longitudinal force and the moment in every segment through stresses by the following formulas:

$$N = \sum_{i=0}^{n} \sigma_i \cdot A_i \quad (9)$$

$$\sigma_{m,i} = \sigma_i - \frac{\sigma_{i,\max} - \sigma_{i,\min}}{2} \quad (10)$$

$$N_{m,i} = \sum_{i=0}^{n} \sigma_{m,i} \cdot A_i \quad (11)$$

$$M = \sum_{i=0}^{n} \sigma_{m,i} \cdot A_i \cdot y_i \quad (12)$$

As a consequence of computing the bending moment *M* and the longitudinal force *N*, a chart of the bearing capacity of the concrete-filled tubular column (see Fig. 2) of 108 mm in the diameter and 4 mm in the thickness of a wall was plotted (sample TB-1). The invented procedure as the program easy for use was automated and presented. To check the bearing capacity of the concrete-filled tubular sample necessity to match the position of the combination of external loads with the plotted bearing capacity curve. If the combination of loads does not extend beyond the load-bearing curve, the ability of the element is secured.

To complete verification of the curve of the bearing capacity (1) Fig. 2a shows the curve of the bearing capacity of a steel tube without concrete filling (2), and a curve of the bearing capacity of the concrete-filled tubular element, where the concrete is reduced to steel with the help of the relation $\delta = f_{ck} / f_y$ (3), and the curve where the concrete is reduced to the steel by the relation $\delta = E_{cm} / E_s$ (4). The Fig. 2b shows the comparison of the curve (1), and the curve, which takes into account the effect of compression of concrete by a steel tube (2) as well as a curve plotted based on experimental tests of comparable samples (3) (Wang, Z. B., et al. 2017 and Huang, W., et al. 2018).These curves were studied, it can be concluded that the reserve bearing capacity is 20% is in the case of compression with zero eccentricity since the effect of compression of concrete by a steel tube, in this case, was not considered.

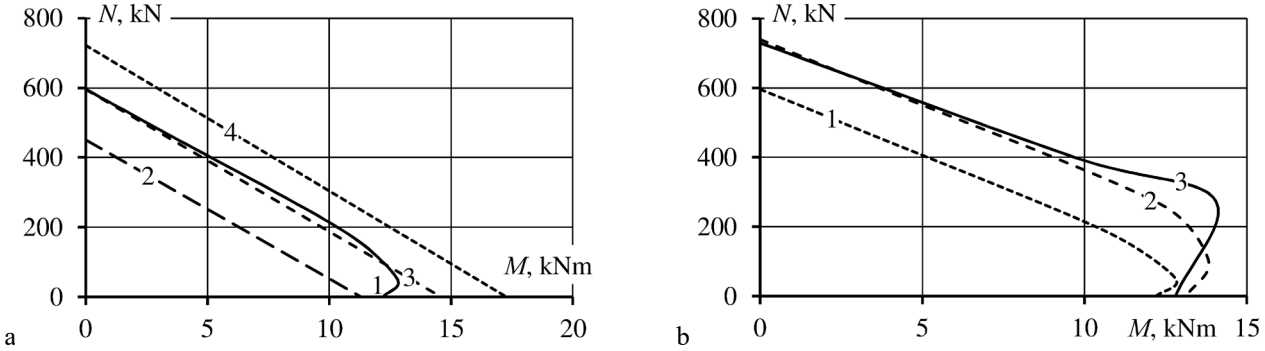

Fig. 2 - Comparison of the bearing capacity *N–M* curve and (a) reduced curves, and (b) experimental curves.

To plot a similar graph of bearing capacity of a jointed element needs to find out the multiplication of the full longitudinal force for every area placed in the tension zone of the concrete-filled tubular element on the corresponding distance from the boundary line to the center of the plot (see Figs. 3 and 4). It is essential to consider the total stretching moment is equal to zero for the load combinations that located at the left of the boundary line 1 (see Fig. 3), consequently, based on the terms of tension the sizes of the joint members are defined based only on constructive requirements.

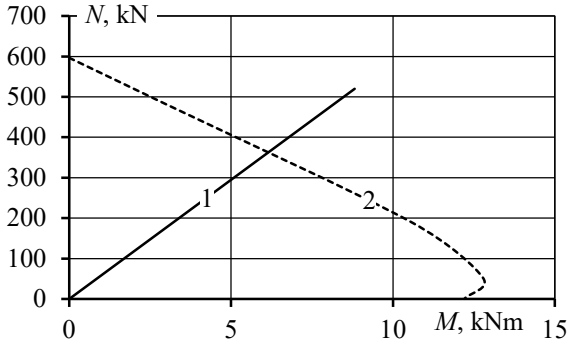

Fig. 3 - The line of constant eccentricity, which shows the appearance of stretching forces at the joint (1) and the curve of bearing capacity *N–M* (2).

To computing the concrete-filled tubular elements on the combinations of external forces placed at the right of the boundary line 1 (Fig. 3) needs to find out the total stretching torque as the multiplication of the tensile strength in every section for the corresponding distance (Fig. 4) from the boundary line to the center of this section $\Sigma(N_t \cdot z_t)$. The multiplication value will vary in proportion to the entire line of action of constant eccentricities 1 (see Fig. 3). Therefore, computing the total stretching torque $\Sigma(N_t \cdot z_t)$ for points on the chart of the bearing capacity of *N–M*, it is essential to consider the fact as during constructing the joint for all combinations of loads the location of which is offside of curve 2 (see Fig. 3), the bearing capacity of the constructed concrete-filled tubular element is insufficient and therefore needs to increase the diameter or the wall thickness of the steel tube (Storozhenko, L. I., 2014; Storozhenko, L. I., & Hasii, H. M., 2015 and Chen, J., Wang, J., & Li, W., 2017)

The chart to finding out the total stretching torque for the dismountable joints of concrete-filled tubular elements equipped with longitudinal ribs showed in Figure 4. After definition $\Sigma(N_t \cdot z_t)$ for the final designing of the joint, bolts and flanges are calculated by the well-known formulas.

The cross-section under the action of the transverse force is calculated by the following formula:

$$\sigma = \frac{Q}{A_{\text{sec}tion}} < f_y \qquad (13)$$

Bolts are calculated by the following formulas:

$$N_b = \frac{\sum (N_t \cdot z_t)}{z_b} \le N_{bs} \qquad (14)$$

$$N_{bs} = R_{bs} A n_s \gamma_b \qquad (15)$$

$$N_{bp} = R_y d \sum t_{\min} \gamma_b \qquad (16)$$

The longitudinal ribs of the joint are calculated by the following formulas:

$$N_r = A_r \cdot R_y \ge N_b \qquad (17)$$

$$\sigma = \frac{M_{\max}}{W_r} \le f_y \qquad (18)$$

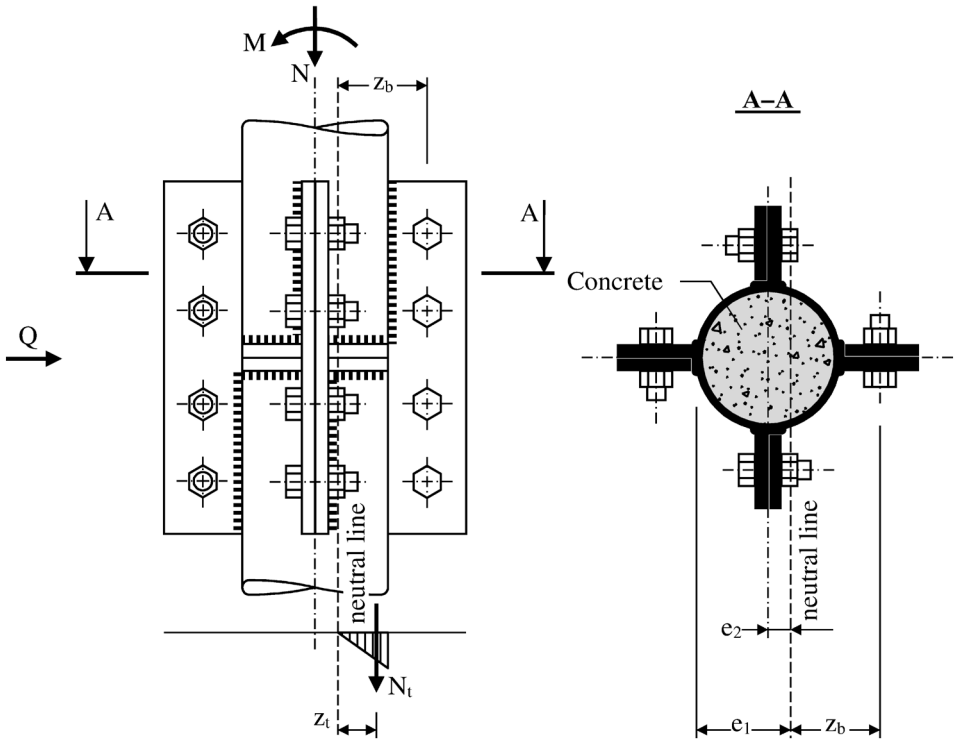

Fig. 4 - Dismountable joints with longitudinal ribs.

By means of the above procedure, Fig. 5 shows a chart of the bearing capacity of a joint equipped with longitudinal ribs, where 1 is a curve of the bearing capacity of the concrete-filled tube of 108 mm in the diameter and 4 mm in the thickness of a wall. The combinations of external loads *N* and *M* that located within the curve 1, satisfy the terms of the bearing capacity of the tube concrete element; 2 – the curve of bearing capacity of 16 bolts of 12 mm in diameter, which applied in the connection. The combination of external loads *N* and *M* that located above line 2 is permissible

based on the condition of the bearing capacity of the bolts; 3 – the curve of the bearing capacity of concrete-filled tubular elements equipped with longitudinal ribs of 200×60×10 mm is similar to curve 1 of the combination of external loads *N* and *M* that is within the curve 1, and satisfies the conditions of bearing capacity.

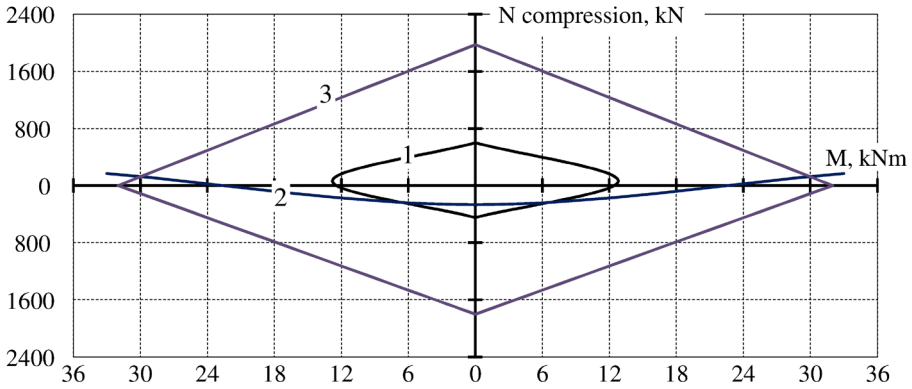

Fig. 5 - Chart of bearing capacity of dismountable joint with longitudinal ribs.

Similarly, a chart of bearing capacity for a dismountable flange joint was plotted and shown in figure 6, where 1 is a curve of the bearing capacity of concrete-filled tubular elements of 108 mm in the diameter and 4 mm in the thickness of a wall. Combinations of external loads *N* and *M*, which are within the curve 1, satisfy the terms of the bearing capacity of the concrete-filled tubular element; 2 – the curve of bearing capacity of 4 bolts of 12 mm in diameter, which applied in the connection. The combination of external loads *N* and *M* that located above line 2 is permissible based on the condition of the bearing capacity of the bolts.

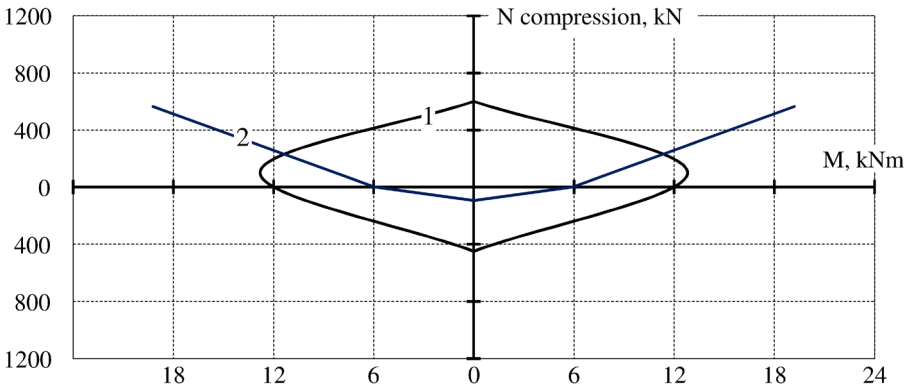

Fig. 6 - Chart of bearing capacity of the dismountable flanged joint.

The stretching force in the bolt is calculated by the following formula:

$$N_b = \frac{\sum(N_t \cdot z_t)}{2 \cdot z_{b2}} \qquad (19)$$

The bolts are checked in tension and against the cutting by the formulas (14–16).
The thickness of the flange is checked based on the following formulas:

$$t_{\min} \geq \sqrt{\frac{6M_1}{bR_y\gamma_c}} \qquad (20)$$

$$t_{\min} \geq \frac{N_{bp}}{R_{bp}d\gamma_b} \qquad (21)$$

Fig. 7 shows the chart of the bearing capacity of the dismountable joints of the concrete-filled tubular elements executed with the help of a steel coupling, where curve 1 is similar as for previous joints, the curve of the bearing capacity of the concrete-filled tubular element of 108 mm in the diameter and 4 mm in the thickness of a wall; curve 2 shows the bearing capacity of a steel coupling of 2.5 mm in thickness and 108 mm in internal diameter. The combinations of external loads of longitudinal force N and bending moment M, which are above this line, satisfy the terms of bearing capacity for the given coupling. The tension in the coupling connection is calculated by the formula proposed by G. Lame:

$$\sigma_2 = \frac{\alpha_0 \cdot G}{(D_m - D) \cdot h} \leq R_y \qquad (22)$$

where G is an external force on the steel coupling which is defined as the ratio of the tensile moment M_{max} up to half the coupling height h and is calculated by Equation:

$$G = \frac{M_{\max}}{0{,}5h} \qquad (23)$$

The section of the element was also tested from the conditions of the transverse force according to Equation:

$$\sigma_1 = \frac{Q}{A} \leq R_y \qquad (24)$$

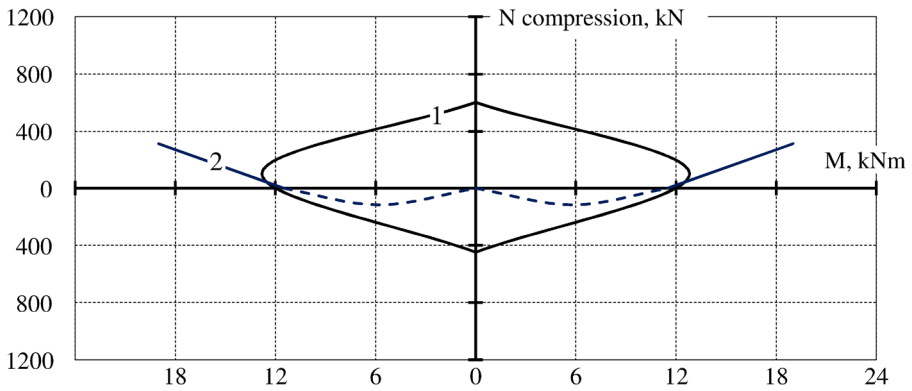

Fig. 7 - Chart of bearing capacity of dismountable joint with a steel coupling.

The investigation was lead for a real structure of a shopping mall, which includes tube columns of 426 mm in outer diameter and 8 mm in the thickness of a wall in order to compare and determine the most optimal joint based on conditions of load-bearing capacity and material costs (Thai, H. T., Uy, B., & Aslani, F., 2017). The comparison was lead under the same loads, namely, the longitudinal force N=1700 kN and the bending moment M=350 kNm. The bearing capacity and dimensions of joints were found out with the proposed methodology. Table 2 shows the results of materials consumption for 1 joint for each type of joints (with a flanged joint – Fig. 8, a joint with longitudinal ribs – Fig. 9 and a coupling connection – Fig. 10) based on conditions of identical bearing capacity. The least cost was found for a dismountable joint equipped with longitudinal ribs, which suggests that for this building, this option is the most optimal.

Table 2 - Cost of steel for the manufacture of 1 joint.

Expenses of materials	Flanged joint N=1700 kN, M=350 kNm	Joint with longitudinal ribs N=1700 kN, M=350 kNm	Joint with steel coupling N=1700 kN, M=350 kNm
Steel, kg	81,7	37,7	43,2
Bolts, pc	8Ø24	16Ø16	4Ø12
Weld seams, mm	2670	3470	4040

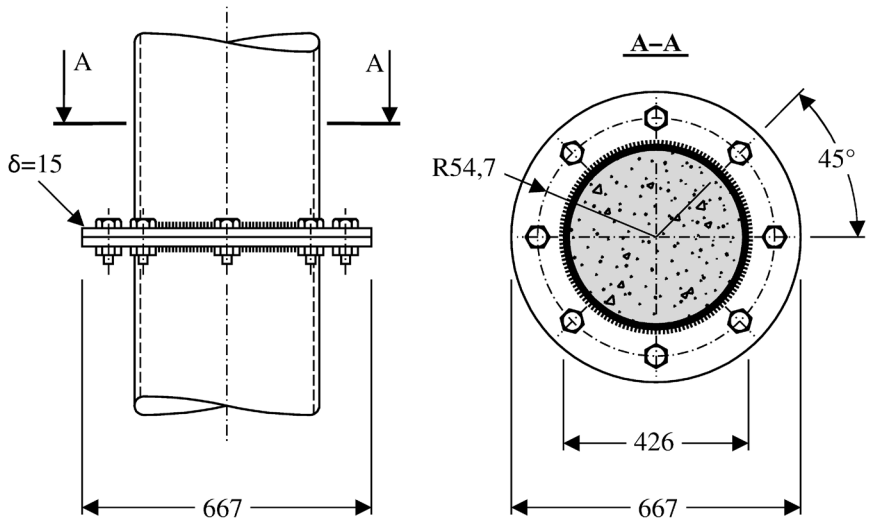

Fig. 8 - Flange joint of concrete-filled tubular elements for the considered combination of loads.

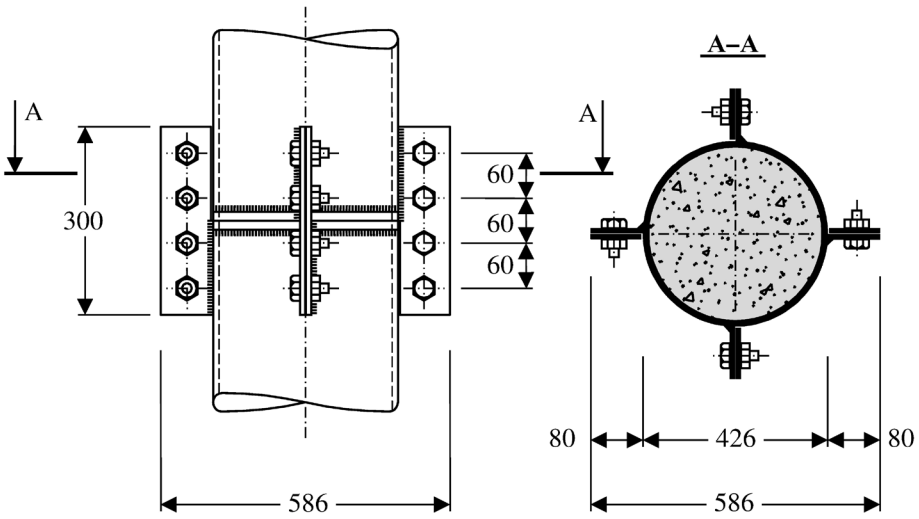

Fig. 9 - The dismountable joint of concrete-filled tubular elements with longitudinal ribs for the considered combination of loads.

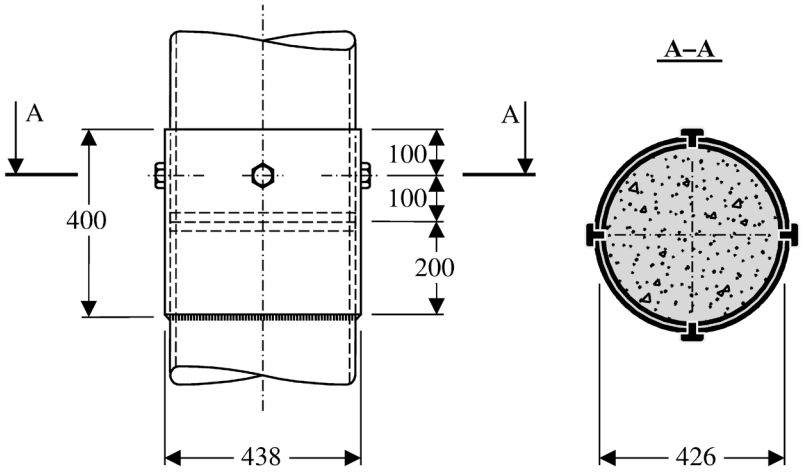

Fig. 10 - The dismountable joint of concrete-filled tubular elements with steel coupling for the considered combination of loads.

3. Conclusion

The paper presents the algorithm for the determination of bearing capacity of concrete-filled tubular elements and their joints by constructing *N–M* curves. The method of determining the bearing capacity of the elements of the dismountable joints is proposed and a comparison was made for the building of the shopping mall, and it was found that for this case, the construction of the joint with longitudinal ribs is the most optimal.

Acknowledgement

The authors would like to thank both Poltava National Technical Yuri Kondratyuk University and Sumy National Agrarian University for make this research possible.

References

Chen, J., Wang, J., & Li, W. (2017). Experimental behaviour of reinforced concrete-filled steel tubes under eccentric tension. *Journal of Constructional Steel Research*, *136*, 91-100

Fam, A., Qie, F. S., & Rizkalla, S. (2004). Concrete filled steel tubes subjected to axial compression and lateral cyclic loads. *Journal of Structural Engineering*, *130*(4), 631-640

Gasii, G. M. (2014). Technological and design features of flat-rod elements with usage of composite reinforced concrete. *Metallurgical and Mining Industry*, *4*, 23-25

Gasii, G., Hasii, O., & Zabolotskyi, O. (2017). Estimate of technical and economic benefits of a new space composite structure. In *MATEC Web of Conferences* (Vol. 116, p. 02014). EDP Sciences. https://doi.org/10.1051/matecconf/201711602014

Gasii G. M. (2017). Structural and design specifics of space grid systems. *Science & Technique*, 16(6), 475-484. https://doi.org/10.21122/2227-1031-2017-16-6-475-484

Hancock, G., Wilkinson, T. J., & Zhao, X. L. (2005). *Cold-formed tubular members and connections: Structural behaviour and design*. Elsevier

Huang, W., Lai, Z., Chen, B., Xie, Z., & Varma, A. H. (2018). Concrete-filled steel tube (CFT) truss girders: Experimental tests, analysis, and design. *Engineering Structures*, *156*, 118-129

Hudz, S., et al. (2018). The Problem of Consideration Torsion Emergence in Beams. *International Journal of Engineering and Technology (UAE)*, 3.2(7), 141-148

Kolokhov, V., et al. (2018). Structure material physic-mechanical characteristics accuracy determination while changing the level of stresses in the structure. *International Journal of Engineering and Technology*, 4.8(7), 75-78

Lai, M. H., & Ho, J. C. M. (2016). A theoretical axial stress-strain model for circular concrete-filled-steel-tube columns. *Engineering Structures*, *125*, 124-143

Semko, P. (2018). Comparison of experimental studies and numerical modeling results of concrete-filled tubular elements with demountable joints. *Industrial Machine Building, Civil Engineering*, 1 (50), 88-97

Semko, P., Skliarenko, S., & Semko, V. (2018). Concrete-filled Tubular Elements Joints Investigation. *International Journal of Engineering and Technology*, 7(3), 494-500

Storozhenko, L. I. (2014). Experimental research of strain-stress state of ferrocement slabs of composite reinforced concrete structure elements. *Metallurgical and Mining Industry*, *6*(6), 40-42

Storozhenko, L. I., & Hasii, H. M. (2015). The new composite designs for mine tunnel support. *Naukovyi Visnyk Natsionalnoho Hirnychoho Universytetu*, 4 (148), 28-34

Tao, Z., Song, T. Y., Uy, B., & Han, L. H. (2016). Bond behavior in concrete-filled steel tubes. *Journal of Constructional Steel Research*, *120*, 81-93

Thai, H. T., Uy, B., & Aslani, F. (2017). Behaviour of bolted endplate composite joints to square and circular CFST columns. *Journal of Constructional Steel Research*, *131*, 68-82

Wang, Z. B., Tao, Z., Han, L. H., Uy, B., Lam, D., & Kang, W. H. (2017). Strength, stiffness and ductility of concrete-filled steel columns under axial compression. *Engineering Structures*, *135*, 209-221

Zeghiche, J., & Chaoui, K. (2005). An experimental behaviour of concrete-filled steel tubular columns. *Journal of Constructional Steel Research*, *61*(1), 53-66